ISME

Vibration Analysis of Coupled Double-Nanocomposite Microplate-systems

A. H. Ghorbanpour-Arani[*]
M.Sc. Student

A. Rastgoo[†]
Professor

H. Vossough[‡]
M.Sc. Student

R. Kolahchi[§]
Assistant Professor

A. Ghorbanpour Arani[**]
Professor

The aim of the paper is to analyze electro-thermo nonlinear vibration of a double-piezoelectric composite microplate-system (DPCMPS) based on nonlocal piezoelasticity theory. The two microplates are assumed to be connected by an enclosing elastic medium which is simulated by Pasternak foundation. Both of smart composite microplates are made of poly-vinylidene fluoride (PVDF) reinforced by zigzag double walled boron nitride nanotubes (DWBNNTs). The micro-electromechanical model is employed to calculate mechanical, thermal and electrical properties of composite. Using nonlinear strain-displacement relations and considering charge equation for coupling between electrical and mechanical fields, the motion equations are derived based on energy method and Hamilton's principle. These equations can't be solved analytically due to their nonlinear terms. Hence, differential quadrature method (DQM) is employed to solve the governing differential equations for the case when all four ends are clamped supported and free electrical boundary condition. The frequency ratio of DPCMPS is investigated for three typical vibrational states, namely, out-of-phase, in-phase and the case when one microplate is fixed in the DPCMPS. A detailed parametric study is conducted to scrutinize the influences of the small scale coefficient, stiffness of the internal elastic medium, the volume fraction and orientation angle of the DWBNNTs reinforcement, temperature change and aspect ratio. The results indicate that with increasing geometrical aspect ratio, the effect of coupling elastic medium between two smart nanocomposite microplates reduces. This study might be useful for the design and smart control of nano/micro devices such as MEMS and NEMS.

Keywords: Nonlinear vibration; Coupled system; Nonlocal piezoelasticity; DWBNNTs.

1 Introduction

Nanocomposites hold the promise of advances that exceed those achieved in recent decades in composite materials. The nanostructure created by a nanophase in polymer matrix represents a radical alternative to the structure of conventional polymer composites. These complex hybrid materials integrate the predominant surfaces of nanoparticles and the polymeric structure into a novel nanostructure, which produces critical fabrication and interface implementations leading to extraordinary properties [1].

[*] M.Sc. Student, University of Tehran, School of Mechanical Engineering, College of Engineering, Tehran, Iran
[†] Professor, University of Tehran, School of Mechanical Engineering, College of Engineering, Tehran, Iran arastgo@ut.ac.ir
[‡]M.Sc. Student, Faculty of Mechanical Engineering, University of Kashan, Kashan, Iran h.vossough@gmail.com
[§] Assistant Professor, Faculty of Mechanical Engineering, University of Kashan, Kashan, Iran r.kolahchi@gmail.com
[**]Corresponding Author, Professor, Faculty of Mechanical Engineering, Institute of Nanoscience & Nanotechnology, University of Kashan, Kashan, Iran aghorban@kashanu.ac.ir

PVDF is an ideal piezoelectric matrix due to characteristics including flexibility in thermoplastic conversion techniques, excellent dimensional stability, abrasion and corrosion resistance, high strength, and capability of maintaining its mechanical properties at elevated temperature. It has therefore found multiple applications in nanocomposites in a wide range of industries including oil and gas, petrochemical, wire and cable, electronics, automotive, and construction. Boron nitride nanotubes (BNNTs) used as the matrix reinforcers, apart from having high mechanical, electrical and chemical properties, present more resistant to oxidation than other conventional nanoreinforcers such as carbon nanotubes (CNTs).
Hence, they are used for high temperature applications [2-5]. Both PVDF and BNNT are smart materials, since they have piezoelectric property.
Piezoelectricity is a classical discipline traced to the original work of Jacques and Pierre Curie around 1880. This phenomenon describes the relations between mechanical strains on a solid and its resulting electrical behavior resulting from changes in the electric polarization. One can create an electrical output from a solid resulting from mechanical strains, or can create a mechanical distortion resulting from the application of an electrical perturbation. Piezoelectric materials have been used to manufacture various sensors, conductors, actuators, etc. in fact, they have become one of the smart materials nowadays [6].
Regarding research development into the use of smart nanocomposite, Mosallaie et al. [7] investigated electro-thermo-mechanical torsional buckling of a piezoelectric polymeric cylindrical shell reinforced by DWBNNTs with an elastic core. They concluded that the higher the in-fill core, the higher is dimensionless critical torsional buckling load. In another research, he and his co-workers [8] studied nonlinear buckling response of embedded piezoelectric cylindrical shell reinforced with BNNT under electro-thermo-mechanical loadings using harmonic differential quadrature method (HDQM). They found that the critical buckling load increases when piezoelectric effect is considered. Ghorbanpour Arani et al. [9] carried out nonlinear vibration and stability of a smart composite micro-tube made of PVDF reinforced by BNNTs embedded in an elastic medium under electro- thermal loadings is investigated. They concluded that stability of the system is strongly dependent on the imposed electric potential and the volume percent of BNNTs reinforcement. Electro-thermo-mechanical nonlinear vibration and instability of a fluid conveying smart composite microtube made of PVDF were investigated by Ghorbanpour Arani et al. [10] based on the modified couple stress theory and Timoshenko beam model. In another work by the same author [11], static stresses analysis of carbon nano-tube reinforced composite (CNTRC) cylinder made of PVDF was investigated.
In recent years, small scale effect in micro- and nano-applications of beam, plate, and shell-type structures has been utilized on the basis of nonlocal elasticity theory which was initiated in the papers of Eringen [12, 13]. He regarded the stress state at a given point as a function of the strain states of all points in the body, while the local continuum mechanics assumes that the stress state at a given point depends uniquely on the strain state at the same point. Ghorbanpour et al. [14] studied Pasternak foundation effect on the axial and torsional waves propagation in the embedded double-walled carbon nanotubes (DWCNTs) using nonlocal elasticity cylindrical shell theory. They concluded that the frequencies are dependent to small scale coefficient and shear modulus of the elastic medium. Ghorbanpour Arani and Jalaei [15] studied transient analysis of simply-supported orthotropic single-layered graphene sheet (SLGS) resting on orthotropic visco-Pasternak foundation subjected to dynamic loads. Wang et al. [16] examined the circumferential nonlocal effect on the buckling and vibration of the carbon nanotubes based on Eringen's nonlocal theory. Vibration behavior of Bilayer graphene sheets in a magnetic field using classic plate theory combined with nonlocal elasticity theory to account for the small-scale effect was investigated by Zhang et al. [17].

The above studies on the nanostructures are on the basis of the nonlocal elasticity theory, which is not proper for a direct use in the piezoelectric materials. Recently, the Eringen's nonlocal elasticity theory was extended by Zhou et al. [18] for the piezoelectric materials. In the nonlocal piezoelectric materials, the stress state and the electric displacement at a given point are, respectively, as a function of the strain state and electric potential of all points in the body. Ke et al. [19] employed nonlocal piezoelasticity model to nonlinear vibration analyze of the piezoelectric nanobeams. They used DQM for study the effects of nonlocal parameter, temperature change and external electric voltage on the nonlinear frequency of the piezoelectric nanobeams. Surface stress and small-scale effects on nonlinear vibration analysis of a single-layer boron nitride sheet were investigated by Ghorbanpour Arai et al. [20] based on theories of nonlocal and surface piezoelasticity. In another work by the same author [21], control and analyze the nonlinear dynamic stability of SLGSs integrated with zinc oxide (ZnO) actuators and sensors were studied based on surface piezoelasticity theory.
With respect to developmental works on mechanical behavior analysis of nano- and micro-plates, it should be noted that none of the researches mentioned above, have considered a coupled double-plate-system. Herein, Murmu and Adhikari [22] analyzed vibration of nonlocal double-nanoplate- system (NDNPS). Their study highlighted that the small-scale effects considerably influence the transverse vibration of NDNPS. Besides, they elucidated that the increase of the stiffness of coupling springs in the NDNPS reduces the small-scale effects during the asynchronous modes of vibration. Also, buckling behavior of the NDNPS was investigated by Murmu et al. [23] who showed that the nonlocal effects in the coupled system are higher within creasing values of the nonlocal parameter for the case of synchronous buckling modes than in the asynchronous buckling modes. Moreover, their analytical results indicated that the increase of the stiffness of the coupling springs in the double-GS-system reduces the nonlocal effects during the asynchronous modes of buckling. Exact solution for nonlocal vibration of double-orthotropic nanoplates embedded in elastic medium was reported by Pouresmaeeli et al. [24] who indicated that the frequency of double-orthotropic nanoplates is always smaller than that of double-isotropic nanoplates. The three papers [22-24] have considered the Winkler model for simulation of elastic medium between two nanoplates. In this simplified model, a proportional interaction between pressure and deflection of SLGS's is assumed, which is carried out in the form of discrete and independent vertical springs. Whereas, Pasternak suggested considering not only the normal stresses but also the transverse shear deformation and continuity among the spring elements, and its subsequent applications for developing the model for buckling analysis, which proved to be more accurate than the Winkler model. Free vibration of viscoelastic double-bonded polymeric nanocomposite plate reinforced by FG-CNTs embedded in viscoelastic foundation was investigated by Mohammadimehr et al. [25].
None of the aforementioned studies [22-25] have considered smart coupled structures while these structures may be used in mechanical behavior control of coupled micro- and nano-structures. Recently, Buckling analysis and smart control of SLGS using elastically coupled PVDF nanoplate using the nonlocal piezoelasticity were studied by Ghorbanpour et al. [26] who showed that the imposed external voltage is an effective controlling parameter for buckling of the SLGS. Moreover, their results indicated that the effect of external voltage becomes more prominent at higher nonlocal parameter and shear modulus. But paper [26] is linear analysis and just one of two plates is smart.
However, to date, no report has been found in the literature on the vibration of an elastically coupled DPCMPS. Motivated by these considerations, in order to improve optimum design of smart microstructure, we aim to study the electro-thermo nonlinear nonlocal vibration of an elastically coupled DPCMPS. Herein, the two PVDF microplates reinforced by DWBNNTs are coupled by an enclosing Pasternak foundation.

Considering the nonlinear strain-displacement relations and charge equation, the nonlinear governing equations are derived using energy method and Hamilton's principle. Hence, the DQM is presented to solve the nonlinear governing equations and estimate the frequency ratio of clamped supported DPCMPS. In present study, the influences of nonlocal parameter, geometrical aspect ratio, temperature gradient, elastic medium constants, orientation angle and volume fraction of DWBNNTs in polymer have been taken into account.

2 Formulation

2.1 Nonlocal piezoelasticity and classical plate theories

2.1.1 Nonlocal piezoelasticity

Based on the theory of nonlocal piezoelasticity, the stress tensor and the electric displacement at a reference point depend not only on the strain components and electric-field components at same position but also on all other points of the body. The nonlocal constitutive behavior for the piezoelectric material can be given as follows [21]:

$$\sigma_{ij}^{nl}(x) = \int_v \alpha(|x-x'|,\tau)\sigma_{ij}^{l} dV(x'), \qquad \forall x \in V \tag{1}$$

$$D_k^{nl} = \int_v \alpha(|x-x'|,\tau) D_k^{l} dV(x'), \qquad \forall x \in V \tag{2}$$

where σ_{ij}^{nl} and σ_{ij}^{l} are, respectively, the nonlocal stress tensor and local stress tensor, D_k^{nl} and D_k^{l} are the components of the nonlocal and local electric displacement. $\alpha(|x-x'|,\tau)$ is the nonlocal modulus. $|x-x'|$ is the Euclidean distance, and $\tau = e_0 a / l$ is defined that l is the external characteristic length, e_0 denotes a constant appropriate to each material, and a is an internal characteristic length of the material. Consequently, $e_0 a$ is a constant parameter which is obtained with molecular dynamics, experimental results, experimental studies and molecular structure mechanics. The constitutive equation of the nonlocal elasticity can be written as [21]:

$$(1-\mu\nabla^2)\sigma_{ij}^{nl} = \sigma_{ij}^{l}, \tag{3}$$

where the parameter $\mu = (e_0 a)^2$ denotes the small scale effect on the response of structures in nano/ micro size, and ∇^2 is the Laplacian operator in the above equation. Similarly, Eq. (2) can be written as [21]:

$$(1-\mu\nabla^2)D_k^{nl} = D_k^{l}, \tag{4}$$

2.1.1 Classical plate theory

Based on the classical plate theory (CPT) which satisfy Kirchhoff assumption, displacement field is expressed as [28]:

$$\begin{aligned} u(x,y,z,t) &= u_0(x,y,t) - z\frac{\partial w_0}{\partial x}, \\ v(x,y,z,t) &= v_0(x,y,t) - z\frac{\partial w_0}{\partial y}, \\ w(x,y,z,t) &= w_0(x,y,t), \end{aligned} \tag{5}$$

where (u,v,w) denote the total displacements of a point along the (x,y,z) coordinates and (u_0,v_0,w_0) are the displacements of points on the mid-plane. The von Kármán nonlinear

strains associated with the above displacement field can be expressed in the following form [28]:

$$\varepsilon_{xx}=\frac{\partial u}{\partial x}+\frac{1}{2}(\frac{\partial w}{\partial x})^2,\quad \varepsilon_{yy}=\frac{\partial v}{\partial y}+\frac{1}{2}(\frac{\partial w}{\partial y})^2,\quad \varepsilon_{xz}=\frac{1}{2}(\frac{\partial u}{\partial z}+\frac{\partial w}{\partial x}),$$
$$\varepsilon_{yz}=\frac{1}{2}(\frac{\partial v}{\partial z}+\frac{\partial w}{\partial y}),\quad \varepsilon_{xy}=\frac{1}{2}(\frac{\partial u}{\partial y}+\frac{\partial v}{\partial x}+\frac{\partial w}{\partial x}\frac{\partial w}{\partial y}),\quad \varepsilon_{zz}=\frac{\partial w}{\partial z}\ , \tag{6}$$

On the basis of the CPT, shear strains $\varepsilon_{xz},\varepsilon_{yz}$ are considered negligible. Hence, the strain equations in terms of the mid-plane displacements are derived by substituting the Eq. (5) into the Eq. (6) as follows

$$\begin{Bmatrix}\varepsilon_{xx}\\ \varepsilon_{yy}\\ \gamma_{xy}\end{Bmatrix}=\begin{Bmatrix}\frac{\partial u_0}{\partial x}+\frac{1}{2}(\frac{\partial w_0}{\partial x})^2\\ \frac{\partial v_0}{\partial y}+\frac{1}{2}(\frac{\partial w_0}{\partial y})^2\\ \frac{\partial u_0}{\partial y}+\frac{\partial v_0}{\partial y}+\frac{\partial w_0}{\partial x}\frac{\partial w_0}{\partial y}\end{Bmatrix}+z\begin{Bmatrix}-\frac{\partial^2 w_0}{\partial x^2}\\ -\frac{\partial^2 w_0}{\partial y^2}\\ -2\frac{\partial^2 w_0}{\partial x\partial y}\end{Bmatrix}, \tag{7}$$

The strain components ε_{xx}, ε_{yy} and γ_{xy} at an arbitrary point of the sheet are related to the middle surface strains and curvatures tensor as follows

$$\begin{Bmatrix}\varepsilon_{xx}\\ \varepsilon_{yy}\\ \gamma_{xy}\end{Bmatrix}=\begin{Bmatrix}\varepsilon^0_{xx}\\ \varepsilon^0_{yy}\\ \gamma^0_{xy}\end{Bmatrix}+z\begin{Bmatrix}\varepsilon^1_{xx}\\ \varepsilon^1_{yy}\\ \gamma^1_{xy}\end{Bmatrix}, \tag{8}$$

where ($\varepsilon^0_{xx},\varepsilon^0_{yy},\gamma^0_{xy}$) are components of the membrane strains (middle surface strains) tensor and ($\varepsilon^1_{xx},\varepsilon^1_{yy},\gamma^1_{xy}$) are components of the bending strain (curvature) tensor.

2.2 Modeling of the problem

An elastically coupled DPCMPS having the length L, the width b and the thickness h, assuming that $h<<l,b$[27], is shown in figure (1). The origin of the Cartesian coordinate system is considered at one corner of the middle surface of the microplate. The x, y and z axes are taken along the length, width, and thickness of the microplates, respectively. The two microplates are made from PVDF and reinforced by DWBNNTs in x-direction so that both microplates are identical. The DPCMPS is subjected to uniform temperature change and polarized in x-direction. The two microplates are coupled by an elastic medium which is simulated by the Pasternak foundation. As is well known this foundation model is characterized by two parameters: the Winkler modulus k_w and shear modulus k_g.

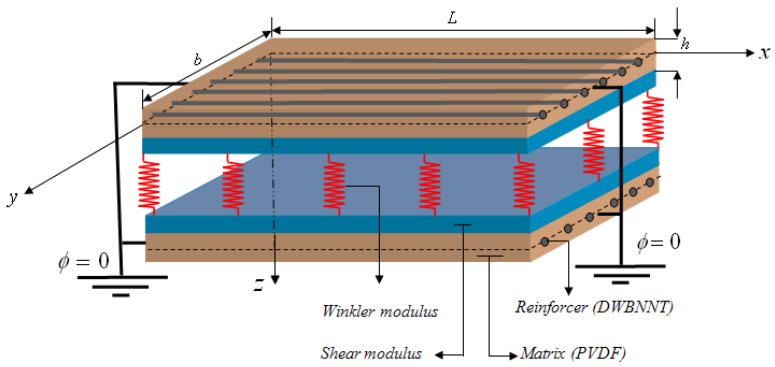

Figure 1 Schematic of double-smart composite microplate-system

2.3 Constitutive equations for piezoelectric materials

In a piezoelectric material, application of an electric field to it will cause a strain proportional to the mechanical field strength, and vice versa. According to a piezoelectric microplate under electro-thermal loads, constitutive equations can be represented as:

$$(1-\mu\nabla^2)\begin{bmatrix}\sigma_{xx}^{nl}\\ \sigma_{yy}^{nl}\\ \sigma_{xy}^{nl}\end{bmatrix}=\begin{bmatrix}\overline{C}_{11} & \overline{C}_{12} & 0\\ \overline{C}_{21} & \overline{C}_{22} & 0\\ 0 & 0 & \overline{C}_{66}\end{bmatrix}\left(\begin{Bmatrix}\varepsilon_{xx}\\ \varepsilon_{yy}\\ \gamma_{xy}\end{Bmatrix}-\begin{pmatrix}\alpha_x\\ \alpha_y\\ 0\end{pmatrix}\Delta T\right)-\begin{bmatrix}e_{11} & 0 & 0\\ e_{12} & 0 & 0\\ 0 & e_{26} & 0\end{bmatrix}\begin{Bmatrix}E_{xx}\\ E_{yy}\\ E_{zz}\end{Bmatrix}, \tag{9}$$

$$(1-\mu\nabla^2)\begin{bmatrix}D_{xx}^{nl}\\ D_{yy}^{nl}\\ D_{xy}^{nl}\end{bmatrix}=\begin{bmatrix}e_{11} & e_{12} & 0\\ 0 & 0 & e_{26}\\ 0 & 0 & 0\end{bmatrix}\left(\begin{Bmatrix}\varepsilon_{xx}\\ \varepsilon_{yy}\\ \gamma_{xy}\end{Bmatrix}-\begin{pmatrix}\alpha_x\\ \alpha_y\\ 0\end{pmatrix}\Delta T\right)-\begin{bmatrix}\in_{11} & 0 & 0\\ 0 & \in_{22} & 0\\ 0 & 0 & \in_{22}\end{bmatrix}\begin{Bmatrix}E_{xx}\\ E_{yy}\\ E_{zz}\end{Bmatrix}, \tag{10}$$

where $e_{ij},\in_{ij}(i,j=1,...,6),\alpha_k(k=x,y)$ and ΔT are piezoelectric constants, dielectric constants, thermal expansion coefficients and temperature gradient, respectively. $\overline{C}_{ij}$ denote transformed stiffness components and is defined as [28]

$$\begin{aligned}\overline{C}_{11}&=C_{11}\cos^4\theta+2(C_{12}+2C_{66})\cos^2\theta\sin^2\theta+C_{22}\sin^4\theta,\\ \overline{C}_{12}&=C_{12}(\cos^4\theta+\sin^4\theta)+(C_{11}+C_{22}-4C_{66})\cos^2\theta\sin^2\theta,\\ \overline{C}_{22}&=C_{22}\cos^4\theta+2(C_{12}+2C_{66})\cos^2\theta\sin^2\theta+C_{11}\sin^4\theta,\\ \overline{C}_{66}&=(C_{11}+C_{22}-2C_{12}-2C_{66})\sin^2\theta\cos^2\theta+C_{66}(\sin^4\theta+\cos^4\theta),\end{aligned} \tag{11}$$

where C_{ij} are components of stiffness tensor. θ is the orientation angle between the global and local Cartesian coordinates, corresponding to the angle between DWBNNTs and the main axis of the matrix.

Electric field tensor E can be written in term of electric potential ϕ as [26]:

$$E=-\nabla\phi. \tag{12}$$

Using approach adopted by Tan and Tong [29] in which they use representative volume element (RVE) based on micro-electro-mechanical models, the mechanical, thermal and electrical properties of the DPCMPS can be obtained from Refs. [9, 29].

2.4 Equations of motion

The governing differential equations of motion are derived using the Hamilton's principle which is given as [25]:

$$\int_0^T (\delta U + \delta V - \delta K)dt = 0 \tag{13}$$

where δU is the virtual strain energy, δV is the virtual work done by external applied forces and δK is the virtual kinetic energy. The motion equations can be derived using Eq. (13) as follows [25]

$$\begin{aligned}
&\frac{\partial N_{xx}}{\partial x} + \frac{\partial N_{xy}}{\partial y} = m_0 \frac{\partial^2 u_0}{\partial t^2}, \\
&\frac{\partial N_{xy}}{\partial x} + \frac{\partial N_{yy}}{\partial y} = m_0 \frac{\partial^2 v_0}{\partial t^2}, \\
&\frac{\partial^2 M_{xx}}{\partial x^2} + 2\frac{\partial^2 M_{xy}}{\partial y \partial x} + \frac{\partial^2 M_{yy}}{\partial y^2} + \frac{\partial}{\partial x}(N_{xx}\frac{\partial w_0}{\partial x} + N_{xy}\frac{\partial w_0}{\partial y}) + \frac{\partial}{\partial y}(N_{xy}\frac{\partial w_0}{\partial x} + N_{yy}\frac{\partial w_0}{\partial y}) \\
&- K_W w_0 + K_G(\frac{\partial^2 w_0}{\partial x^2} + \frac{\partial^2 w_0}{\partial y^2}) + q = m_0 \frac{\partial^2 w_0}{\partial t^2} - m_2 \frac{\partial^2}{\partial t^2}(\frac{\partial^2 w_0}{\partial x^2} + \frac{\partial^2 w_0}{\partial y^2}),
\end{aligned} \tag{14}$$

where

$$(m_0, m_2) = \int_{-h/2}^{h/2} \rho_0 (1, z^2) dz \tag{15}$$

where (m_0, m_2) are mass moments of inertia and ρ_0 denotes the density of the material. Meanwhile, the force resultants (N_{xx}, N_{yy}, N_{xy}) and the moment resultants (M_{xx}, M_{yy}, M_{xy}) of plate can be defined as

$$\{(N_x, N_y, N_{xy}), (M_x, M_y, M_{xy})\} = \int_{-h/2}^{h/2} \{\sigma_x, \sigma_y, \tau_{xy}\}(1, z) dz \tag{16}$$

Charge equation for coupling electrical and mechanical fields is [26]

$$\frac{\partial D_x}{\partial x} + \frac{\partial D_y}{\partial y} + \frac{\partial D_z}{\partial z} = 0, \tag{17}$$

In this study, transverse vibration is investigated (i.e. $u_0 = v_0 = 0$). Considering $w_0(x, y, t) = W(x, y)e^{i\omega t}$ and defining dimensionless parameters as follows

$$\begin{aligned}
&\beta_x = \frac{h}{l}, \quad \beta_y = \frac{h}{b}, \quad Q_1 = \frac{\overline{C}_{12}}{\overline{C}_{11}}, \quad Q_2 = \frac{\overline{C}_{22}}{\overline{C}_{11}}, \quad Q_3 = \frac{\overline{C}_{66}}{\overline{C}_{11}}, \quad T_x = \alpha_{xx} T, \\
&T_y = \alpha_{yy} T, \quad K_G^* = \frac{k_g}{\overline{C}_{11} l}, \quad K_W^* = \frac{k_w l}{\overline{C}_{11}}, \quad \overline{m}_0 = \frac{m_0}{\rho_0 l}, \quad \overline{m}_2 = \frac{m_2}{\rho_0 l^3}, \\
&\Omega = \omega l \sqrt{\frac{\rho_0}{\overline{C}_{11}}}, \quad \phi_0 = l\sqrt{\frac{\overline{C}_{11}}{\in_{11}}}, \quad \overline{e}_1 = \frac{e_{11}\phi_0}{\overline{C}_{11} l} = \frac{e_{11}}{\sqrt{\overline{C}_{11} \in_{11}}}, \\
&\overline{e}_2 = \frac{e_{12}\phi_0}{\overline{C}_{11} l} = \frac{e_{12}}{\sqrt{\overline{C}_{11} \in_{11}}}, \quad \overline{e}_3 = \frac{e_{26}\phi_0}{\overline{C}_{11} l} = \frac{e_{26}}{\sqrt{\overline{C}_{11} \in_{11}}}, \quad \mu^* = \frac{\mu}{l^2}, \\
&\zeta = \frac{x}{l}, \quad \eta = \frac{y}{b}, \quad W^* = \frac{W}{h}, \quad \Phi = \frac{\phi}{\phi_0},
\end{aligned} \tag{18}$$

As well as substituting combination of Eqs. (5)-(12) and (15)-(16) into Eqs. (14) and (17), the dimensionless nonlinear nonlocal motion equations of DPCMPS can be written as

$$\frac{-1}{12}\beta_x^4\frac{\partial^4 W_{(m)}^*}{\partial\zeta^4}-\frac{1}{6}\beta_x^2\beta_y^2(Q_1+2Q_3)\frac{\partial^4 W_{(m)}^*}{\partial\eta^2\partial\zeta^2}-\frac{1}{12}Q_2\beta_y^4\frac{\partial^4 W_{(m)}^*}{\partial\eta^4}- \tag{19}$$
$$(T_x+Q_1T_y)\beta_x^2\frac{\partial^2 W_{(m)}^*}{\partial\zeta^2}+\beta_x^2\bar{e}_1\frac{\partial^2 W_{(m)}^*}{\partial\zeta^2}\frac{d\Phi_{(m)}}{d\zeta}+\beta_y^2(Q_1T_x+Q_2T_y)\frac{\partial^2 W_{(m)}^*}{\partial\eta^2}+$$
$$\beta_y^2\bar{e}_2\frac{\partial^2 W_{(m)}^*}{\partial\eta^2}\frac{d\Phi_{(m)}}{d\eta}+\Omega^2\Bigg[\overline{m}_0\beta_x W_{(m)}^*-(\mu^*\overline{m}_0+\overline{m}_2)(\beta_x\frac{\partial^2 W_{(m)}^*}{\partial\zeta^2}+\frac{\beta_y^2}{\beta_x}\frac{\partial^2 W_{(m)}^*}{\partial\eta^2})$$
$$+\mu^*\overline{m}_2(\beta_x\frac{\partial^4 W_{(m)}^*}{\partial\zeta^4}+2\frac{\beta_y^2}{\beta_x}\frac{\partial^4 W_{(m)}^*}{\partial\eta^2\partial\zeta^2}+\frac{\beta_y^4}{\beta_x^3}\frac{\partial^4 W_{(m)}^*}{\partial\eta^4})\Bigg]+F_{(m)}=0,\quad (m)=1,2$$

$$\beta_x^4\bar{e}_1(\frac{\partial W_{(m)}^*}{\partial\zeta}\frac{\partial^2 W_{(m)}^*}{\partial\zeta^2})+\bar{e}_2\beta_x^2\beta_y^2(\frac{\partial W_{(m)}^*}{\partial\eta}\frac{\partial^2 W_{(m)}^*}{\partial\eta\partial\zeta})+\bar{e}_3\beta_x^2\beta_y^2(\frac{\partial W_{(m)}^*}{\partial\eta}\frac{\partial^2 W_{(m)}^*}{\partial\eta\partial\zeta}+ \tag{20}$$
$$\frac{\partial W_{(m)}^*}{\partial\zeta}\frac{\partial^2 W_{(m)}^*}{\partial\eta^2})-\beta_x^2\frac{d^2\Phi_{(m)}}{d\zeta^2}=0,\quad (m)=1,2$$

where

$$F_1=+\mu^*K_W^*\Bigg(\beta_x(\frac{\partial^2 W_{(1)}^*}{\partial\zeta^2}-\frac{\partial^2 W_{(2)}^*}{\partial\zeta^2})+\frac{\beta_y^2}{\beta_x}(\frac{\partial^2 W_{(1)}^*}{\partial\eta^2}-\frac{\partial^2 W_{(2)}^*}{\partial\eta^2})\Bigg)-$$
$$\mu^*K_G^*\Bigg(\beta_x(\frac{\partial^4 W_{(1)}^*}{\partial\zeta^4}-\frac{\partial^4 W_{(2)}^*}{\partial\zeta^4})+2\frac{\beta_y^2}{\beta_x}(\frac{\partial^4 W_{(1)}^*}{\partial\eta^2\partial\zeta^2}-\frac{\partial^4 W_{(2)}^*}{\partial\eta^2\partial\zeta^2})+\frac{\beta_y^4}{\beta_x^3}(\frac{\partial^4 W_{(1)}^*}{\partial\zeta^4}-\frac{\partial^4 W_{(2)}^*}{\partial\zeta^4})\Bigg) \tag{21}$$
$$-K_W^*\beta_x(W_{(1)}^*-W_{(2)}^*)+K_G^*\Bigg(\beta_x(\frac{\partial^2 W_{(1)}^*}{\partial\zeta^2}-\frac{\partial^2 W_{(2)}^*}{\partial\zeta^2})+\frac{\beta_y^2}{\beta_x}(\frac{\partial^2 W_{(1)}^*}{\partial\eta^2}-\frac{\partial^2 W_{(2)}^*}{\partial\eta^2})\Bigg),$$
$$F_2=\mu^*K_W^*\Bigg(\beta_x(\frac{\partial^2 W_{(2)}^*}{\partial\zeta^2}-\frac{\partial^2 W_{(1)}^*}{\partial\zeta^2})+\frac{\beta_y^2}{\beta_x}(\frac{\partial^2 W_{(2)}^*}{\partial\eta^2}-\frac{\partial^2 W_{(1)}^*}{\partial\eta^2})\Bigg)-$$
$$\mu^*K_G^*\Bigg(\beta_x(\frac{\partial^4 W_{(2)}^*}{\partial\zeta^4}-\frac{\partial^4 W_{(1)}^*}{\partial\zeta^4})+2\frac{\beta_y^2}{\beta_x}(\frac{\partial^4 W_{(2)}^*}{\partial\eta^2\partial\zeta^2}-\frac{\partial^4 W_{(1)}^*}{\partial\eta^2\partial\zeta^2})+\frac{\beta_y^4}{\beta_x^3}(\frac{\partial^4 W_{(2)}^*}{\partial\zeta^4}-\frac{\partial^4 W_{(1)}^*}{\partial\zeta^4})\Bigg)$$
$$-K_W^*\beta_x(W_{(2)}^*-W_{(1)}^*)+K_G^*\Bigg(\beta_x(\frac{\partial^2 W_{(2)}^*}{\partial\zeta^2}-\frac{\partial^2 W_{(1)}^*}{\partial\zeta^2})+\frac{\beta_y^2}{\beta_x}(\frac{\partial^2 W_{(2)}^*}{\partial\eta^2}-\frac{\partial^2 W_{(1)}^*}{\partial\eta^2})\Bigg),$$

where subscript (1) and (2) denote the upper and the lower microplates, respectively. The clamped supported mechanical and free electrical boundary conditions can be expressed as

$$W_{(m)}^*=0,\ \partial W_{(m)}^*/\partial\zeta=0\ \text{ at edges }\ \zeta=0\ \text{ and }\ \zeta=1$$
$$W_{(m)}^*=0,\ \partial W_{(m)}^*/\partial\zeta=0\ \text{ at edges }\ \eta=0\ \text{ and }\ \eta=1 \tag{22}$$

2.5 Vibrational states of DPCMPS

In this paper, vibrational states of DPCMPS including out-of-phase sequence, in-phase sequence, and one-microplate being stationary as shown in figures (2a), (2b), and (2c), are discussed, respectively.

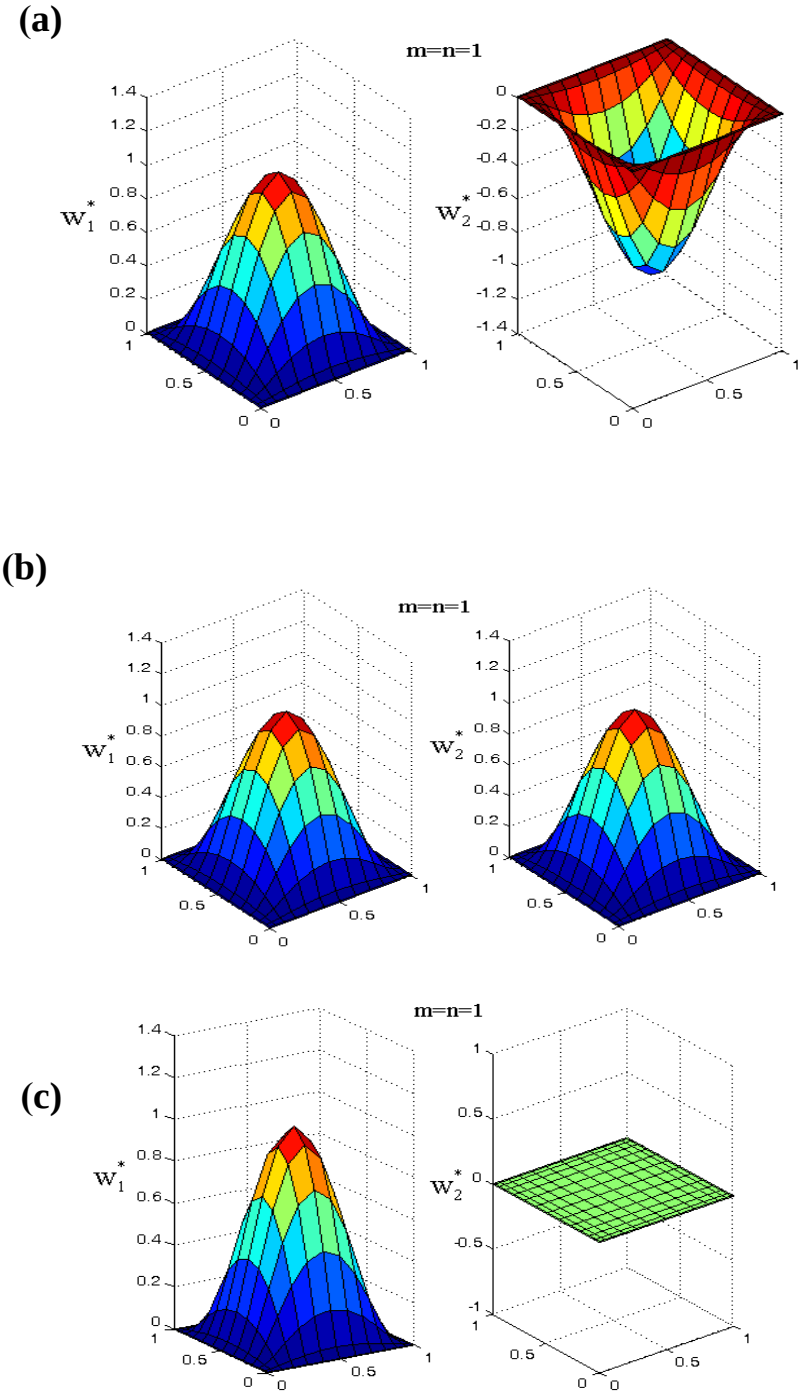

Figure 2 Vibrational states of DSCMPS; (a) out-of-phase vibration, (b) in-phase vibration, (c) one microplate fixed

2.5.1 Out-of-phase vibration

In this case, both microplates vibrate asynchronously, and $W_{(1)}^* - W_{(2)}^* \neq 0$, as shown in figure (2a) for first mode.

2.5.2 In-phase vibration

In this case, both microplates vibrate synchronously, hence the relative displacement between them disappear ($W^*_{(1)} = W^*_{(2)}$), as shown in figure (2b) for first mode. Thus, any one of the two microplates could represent the vibration of the coupled system.

2.5.3 One microplate being stationary

In this case, one microplate is fixed in the DPCMPS (i.e. $W^*_{(2)} = 0$), as shown in figure (2c) for first mode. In mentioned case, the DPCMPS behaves as if upper microplate is embedded in Pasternak foundation.

Generally, Since there are nonlinear terms in governing equations, we can't obtain natural frequency for all mentioned cases similar to the references [22-24] analytically. Therefore, we performed the aforementioned conditions in computer code which written by MATLAB software based on DQ method.

2.6 DQ method

As can be seen the coupled governing equations contain nonlinear terms and should be solved using a numerical method such as DQM. In this method, the differential equations are changed into a first order algebraic equation by employing appropriate weighting coefficients. Weighting coefficients do not relate to any special problem and only depend on the grid spacing. For implementation of the DQ approximation, consider a function $f(\zeta,\eta)$ which has the field on a rectangular domain ($0 \le \zeta \le 1$ and $0 \le \eta \le 1$) with $n_\zeta \times n_\eta$ grid points along x and y axes. According to DQ method, the r[th] derivative of a function $f(x,y)$ can be defined as [30]:

$$\left.\frac{\partial^r f(\zeta,\eta)}{\partial \zeta^r}\right|_{(\zeta,\eta)=(\zeta_i,\eta_j)} = \sum_{m=1}^{n_\zeta} C_{im}^{\zeta(r)} f(\zeta_m,\eta_j) = \sum_{m=1}^{n_x} C_{im}^{\zeta(r)} f_{mj}, \quad \begin{cases} i = 1,2,...,n_\zeta \\ j = 1,2,...,n_\eta \\ r = 1,2,...,n_\zeta - 1 \end{cases} \tag{23}$$

where C_{ij}^{ζ} are weighting coefficients and defined as:

$$C_{ij}^{\zeta} = \begin{cases} \dfrac{M(\zeta_i)}{(\zeta_i - \zeta_j)M(\zeta_j)} & for \ \ i \neq j \\ -\sum\limits_{\substack{j=1 \\ i \neq j}}^{n_\zeta} C_{ij}^{\zeta} & for \ \ i = j \end{cases}, \tag{24}$$

where $M(\zeta_i)$ is Lagrangian operators which can be presented as:

$$M(\zeta_i) = \prod_{\substack{j=1 \\ i \neq j}}^{n_\zeta} (\zeta_i - \zeta_j). \tag{25}$$

The weighting coefficients for the second, third and fourth derivatives are defined as:

$$C_{ij}^{\zeta(2)}=\sum_{k=1}^{n_\zeta}C_{ik}^{\zeta(1)}C_{kj}^{\zeta(1)},\quad C_{ij}^{\zeta(3)}=\sum_{k=1}^{n_\zeta}C_{ik}^{\zeta(1)}C_{kj}^{\zeta(2)}=\sum_{k=1}^{n_\zeta}C_{ik}^{\zeta(2)}C_{kj}^{\zeta(1)}$$
$$C_{ij}^{\zeta(4)}=\sum_{k=1}^{n_\zeta}C_{ik}^{\zeta(1)}C_{kj}^{\zeta(3)}=\sum_{k=1}^{n_\zeta}C_{ik}^{\zeta(3)}C_{kj}^{\zeta(1)}. \tag{26}$$

In a similar method, the weighting coefficients for y-direction can be obtained. The coordinates of grid points are chosen as:

$$\zeta_i=\frac{1}{2}\left[1-\cos(\frac{\pi(i-1)}{(n_x-1)})\right],\eta_j=\frac{1}{2}\left[1-\cos(\frac{\pi(j-1)}{(n_y-1)})\right]. \tag{27}$$

The motion equations using DQM can be rewritten as:

$$\begin{aligned}
&-\frac{1}{12}\beta_x^4(\sum_{k=1}^{n_x}C_{i,k}^{\zeta(4)}W_{(m)k,j}^*)-\frac{1}{6}\beta_x^2\beta_y^2(Q_1+2Q_3)(\sum_{k_1=1}^{n_x}\sum_{k_2=1}^{n_y}C_{i,k_1}^{\zeta(2)}C_{j,k_2}^{\eta(2)}W_{(m)k_1,k_2}^*)-\frac{1}{12}Q_2\beta_y^4(\sum_{k=1}^{n_y}C_{j,k}^{\eta(4)}W_{(m)i,k}^*)\\
&-(T_x+Q_1T_y)\beta_x^2(\sum_{k=1}^{n_x}C_{i,k}^{\zeta(2)}W_{(m)k,j}^*)+\beta_x^2\bar{e}_1(\sum_{k=1}^{n_x}C_{i,k}^{\zeta(2)}W_{(m)k,j}^*)(\sum_{k=1}^{n_x}C_{i,k}^{\zeta(1)}\Phi_{(m)k,j})+\beta_y^2(Q_1T_x+Q_2T_y)\\
&(\sum_{k=1}^{n_y}C_{j,k}^{\eta(2)}W_{(m)i,k}^*)+\beta_y^2\bar{e}_2(\sum_{k=1}^{n_y}C_{j,k}^{\eta(2)}W_{(m)_{i,k}}^*)(\sum_{k=1}^{n_x}C_{i,k}^{\zeta(1)}\Phi_{(m)k,j})\\
&+\Omega^2\Big[\overline{m}_0\beta_xW_{(m)i,j}^*-(\mu^*\overline{m}_0+\overline{m}_2)(\beta_x(\sum_{k=1}^{n_x}C_{i,k}^{\zeta(2)}W_{(m)k,j}^*)+\frac{\beta_y^2}{\beta_x}(\sum_{k=1}^{n_y}C_{j,k}^{\eta(2)}W_{(m)i,k}^*))\\
&-\mu^*\overline{m}_2(\beta_x(\sum_{k=1}^{n_x}C_{i,k}^{\zeta(4)}W_{(m)k,j}^*)+2\frac{\beta_y^2}{\beta_x}(\sum_{k_1=1}^{n_x}\sum_{k=1}^{n_y}C_{i,k_1}^{\zeta(2)}C_{j,k_2}^{\eta(2)}W_{(m)k_1,k_2}^*)+\frac{\beta_y^4}{\beta_x^3}(\sum_{k=1}^{n_y}C_{j,k}^{\eta(4)}W_{(m)i,k}^*)\Big]=0
\end{aligned} \tag{28}$$

$$\begin{aligned}
&\beta_x^4\bar{e}_1((\sum_{k=1}^{n_x}C_{i,k}^{\zeta(1)}W_{(m)k,j}^*)(\sum_{k=1}^{n_x}C_{i,k}^{\zeta(2)}W_{(m)k,j}^*))+\bar{e}_2\beta_x^2\beta_y^2((\sum_{k=1}^{n_y}C_{j,k}^{\eta(1)}W_{(m)i,k}^*)(\sum_{k_1=1}^{n_x}\sum_{k=1}^{n_y}C_{i,k_1}^{\zeta(1)}C_{j,k_2}^{\eta(1)}W_{(m)k_1,k_2}^*))\\
&+\bar{e}_3\beta_x^2\beta_y^2((\sum_{k=1}^{n_y}C_{j,k}^{\eta(1)}W_{(m)i,k}^*)(\sum_{k_1=1}^{n_x}\sum_{k=1}^{n_y}C_{i,k_1}^{\zeta(1)}C_{j,k_2}^{\eta(1)}W_{(m)k_1,k_2}^*)+(\sum_{k=1}^{n_x}C_{i,k}^{\zeta(1)}W_{(m)k,j}^*)(\sum_{k=1}^{n_y}C_{j,k}^{\eta(4)}W_{(m)i,k}^*))\\
&+\beta_x^2(\sum_{k=1}^{n_x}C_{i,k}^{\zeta(2)}\Phi_{(m)k,j})=0
\end{aligned} \tag{29}$$

where

$$
\begin{aligned}
F_1 &= +\mu^* K_W^* \Big(\beta_x \Big(\sum_{k=1}^{n_x} C_{i,k}^{\zeta(2)} W_{(1)k,j}^* - \sum_{k=1}^{n_x} C_{i,k}^{\zeta(2)} W_{(2)k,j}^*\Big) + \frac{\beta_y^2}{\beta_x}\Big(\sum_{k=1}^{n_y} C_{j,k}^{\eta(2)} W_{(1)i,k}^* - \sum_{k=1}^{n_y} C_{j,k}^{\eta(2)} W_{(2)i,k}^*\Big)\Big) \\
&- \mu^* K_G^* \Big(\beta_x \Big(\sum_{k=1}^{n_x} C_{i,k}^{\zeta(4)} W_{(1)k,j}^* - \sum_{k=1}^{n_x} C_{i,k}^{\zeta(4)} W_{(2)k,j}^*\Big) + 2\frac{\beta_y^2}{\beta_x}\Big(\sum_{k_1=1}^{n_x}\sum_{k=1}^{n_y} C_{i,k_1}^{\zeta(2)} C_{j,k_2}^{\eta(2)} W_{(1)k_1,k_2}^* \\
&- \sum_{k_1=1}^{n_x}\sum_{k=1}^{n_y} C_{i,k_1}^{\zeta(2)} C_{j,k_2}^{\eta(2)} W_{(2)k_1,k_2}^*\Big) + \frac{\beta_y^4}{\beta_x^3}\Big(\sum_{k=1}^{n_y} C_{j,k}^{\eta(4)} W_{(1)i,k}^* - \sum_{k=1}^{n_y} C_{j,k}^{\eta(4)} W_{(2)i,k}^*\Big)\Big) \\
&- K_W^* \beta_x (W_{(1)i,j}^* - W_{(2)i,j}^*) + K_G^* \Big(\beta_x \Big(\sum_{k=1}^{n_x} C_{i,k}^{\zeta(2)} W_{(1)k,j}^* - \sum_{k=1}^{n_x} C_{i,k}^{\zeta(2)} W_{(2)k,j}^*\Big) + \\
&\frac{\beta_y^2}{\beta_x}\Big(\sum_{k=1}^{n_y} C_{j,k}^{\eta(2)} W_{(1)i,k}^* - \sum_{k=1}^{n_y} C_{j,k}^{\eta(2)} W_{(2)i,k}^*\Big)\Big)
\end{aligned}
\tag{30}
$$

$$
\begin{aligned}
F_2 &= +\mu^* K_W^* \Big(\beta_x \Big(\sum_{k=1}^{n_x} C_{i,k}^{\zeta(2)} W_{(2)k,j}^* - \sum_{k=1}^{n_x} C_{i,k}^{\zeta(2)} W_{(1)k,j}^*\Big) + \frac{\beta_y^2}{\beta_x}\Big(\sum_{k=1}^{n_y} C_{j,k}^{\eta(2)} W_{(2)i,k}^* - \sum_{k=1}^{n_y} C_{j,k}^{\eta(2)} W_{(1)i,k}^*\Big)\Big) \\
&- \mu^* K_G^* \Big(\beta_x \Big(\sum_{k=1}^{n_x} C_{i,k}^{\zeta(4)} W_{(2)k,j}^* - \sum_{k=1}^{n_x} C_{i,k}^{\zeta(4)} W_{(1)k,j}^*\Big) + 2\frac{\beta_y^2}{\beta_x}\Big(\sum_{k_1=1}^{n_x}\sum_{k=1}^{n_y} C_{i,k_1}^{\zeta(2)} C_{j,k_2}^{\eta(2)} W_{(2)k_1,k_2}^* \\
&- \sum_{k_1=1}^{n_x}\sum_{k=1}^{n_y} C_{i,k_1}^{\zeta(2)} C_{j,k_2}^{\eta(2)} W_{(1)k_1,k_2}^*\Big) + \frac{\beta_y^4}{\beta_x^3}\Big(\sum_{k=1}^{n_y} C_{j,k}^{\eta(4)} W_{(2)i,k}^* - \sum_{k=1}^{n_y} C_{j,k}^{\eta(4)} W_{(1)i,k}^*\Big)\Big) \\
&- K_W^* \beta_x (W_{(2)i,j}^* - W_{(1)i,j}^*) + K_G^* \Big(\beta_x \Big(\sum_{k=1}^{n_x} C_{i,k}^{\zeta(2)} W_{(2)k,j}^* - \sum_{k=1}^{n_x} C_{i,k}^{\zeta(2)} W_{(1)k,j}^*\Big) + \\
&\frac{\beta_y^2}{\beta_x}\Big(\sum_{k=1}^{n_y} C_{j,k}^{\eta(2)} W_{(2)i,k}^* - \sum_{k=1}^{n_y} C_{j,k}^{\eta(2)} W_{(1)i,k}^*\Big)\Big)
\end{aligned}
$$

In order to carry out the eigenvalue analysis, the domain and boundary points are separated and in vector forms they are denoted as {d} and {b}, respectively. Hence, the discretized form of the motion equations (Eqs. (28)–(30)) together with the boundary conditions (Eqs. (22)) can be expressed in matrix form as

$$
\left(\underbrace{\left[K_L + K_{NL}\right]}_{[K]} - \Omega^2 \left[M\right] \right) \begin{bmatrix} \{d\} \\ \{b\} \end{bmatrix} = 0, \tag{31}
$$

in which $[M]$, $[K_L]$ and $[K_{NL}]$ are the mass matrix, linear stiffness matrix and nonlinear stiffness matrix. This nonlinear equation can now be solved using a direct iterative process as follows:

- First , nonlinearity is ignored by taking $[K_{NL}] = 0$ to solve the eigenvalue problem expressed in equation (31). This yields the linear eigenvalue (Ω_L) and associated eigenvector. The eigenvector is then scaled up so that the maximum transverse displacement of the microplate is equal to the maximum eigenvector, i.e. the given vibration amplitude $W_{\max}^*$.
- Using linear eigenvector, $[K_{NL}]$ could be evaluated. Eigenvalue problem is then solved by substituting $[K_{NL}]$ into equation (31). This would give the nonlinear eigenvalue (Ω_{NL}) and the new eigenvector.

- The new nonlinear eigenvector is scaled up again and the above procedure is repeated iteratively until the frequency values from the two subsequent iterations ' r ' and ' $r+1$ ' satisfy the prescribed convergence criteria [30] as

$$\frac{\left|\omega^{r+1}-\omega^{r}\right|}{\omega^{r}}<\varepsilon_0 \tag{32}$$

where ε_0 is a small value number and in the present analysis it is taken to be 0.1%.

3 Numerical results and discussion

Mechanical, thermal and electrical properties of PVDF matrix and DWBNNT reinforcement are presented in Table (1) [10]. The final converged solution using the numerical procedure outlined in Section 2.6 above is illustrated as the influences of the elastic medium, nonlocal parameter, aspect ratio, temperature change on the frequency ratio of the DPCMPS. The frequency ratio is defined as

$$\text{Frequency Ratio}=\frac{\Omega_{NL}}{\Omega_{L}},$$

where Ω_{NL} and Ω_{L} are the nonlinear and linear frequencies of the DPCMPS, respectively.
Since, no reference to such a work is found to-date in the literature, its validation is not possible. However, the present work could be partially validated based on a simplified analysis suggested by Shen et al. [15] on thermal nonlinear vibration of the SLGS for which the coupled plate and volume percent of DWBNNT in polymer were ignored. For this purpose, a SLGS with $\rho=0$, $T=300\,K$, $L=9.496\,nm$, $b=4.877\,nm$, $h=0.145\,nm$, $\rho_0=5624\ kg/m^3$, $K_w=K_G=0$ and $e_0a=0.67\,nm$ is considered.

Table (2) illustrates the result of validation exercise by showing nonlinear-to-linear frequency for different dimensionless amplitude and temperature. As can be seen, the results obtained are in good agreement with those expressed in [15].
In order to show the effect of dimensionless coupling elastic medium between two smart composite microplates, the frequency ratio (Ω_{NL}/Ω_{L}) versus the dimensionless maximum amplitude ($W^{*}_{\max}$) is demonstrated in figures (3a)-(3d) for three different cases of vibration characteristic. These cases are:

Table 1 Mechanical, electrical, and thermal properties of PVDF and DBNNT

PVDF	DBNNT
$C_{11}=238.24(Gpa)$	$E=1.8(Tpa)$
$C_{22}=23.6(GPa)$	$\upsilon=0.34$
$C_{12}=3.98(GPa)$	$e_{11}=0.95(C/m^2)$
$C_{66}=6.43(GPa)$	$\alpha_x=1.2e-6(1/K)$
$e_{11}=-0.135(C/m^2)$	$\alpha_y=0.6e-6(1/K)$
$e_{12}=-0.145(C/m^2)$	
$\in=1.1068\times10^{-8}(F/m)$	
$\alpha_x=7.1e-5(1/K)$	
$\alpha_y=7.1e-5(1/K)$	

Case 1: Out-of-phase (asynchronous) vibration.
Case 2: Vibration with one smart composite microplate fixed.
Case 3: In-phase (synchronous) vibration.

Noted that the coupling elastic medium in this study is simulated as spring constants of Winkler-type (K_W^*) and shear constants of Pasternak-type (K_G^*). In general, the frequency ratio decreases with increasing elastic medium constants. This is because increasing Winkler and Pasternak coefficients increases the system stiffness. In addition, the difference between three cases becomes remarkable with increasing values of stiffness parameter. The frequency ratio of cases 1 and 2 decreases with increasing elastic medium constants. Furthermore, Ω_{NL}/Ω_L for case 2 is higher than case 1 because in case 2, the DPCMPS treats as a single smart composite microplate with the elastic foundation effect.
Therefore, the stiffness of the system in case 2 is lower than case 1 and consequently, its frequency ratio is higher with respect to case 1. It is also worth mentioning that the frequency ratio of case 3 is independent of elastic medium stiffness. It is due to the fact that in the case of in-phase vibration, the DPCMPS acts as a single smart composite microplate without the internal elastic foundation effect. Figures (4a)-(4d) demonstrates the effects of dimensionless nonlocal parameter (μ^*) on the frequency ratio versus the dimensionless maximum amplitude for three cases of out-of-phase vibration, vibration with one microplate fixed and in-phase vibration.
It should be noted that the nonlocal parameter $\mu^* = 0$ corresponds to the classical microplate without the nonlocal effect. As can be seen, the frequency ratio for the case of in-phase vibration is higher than cases of out-of-phase vibration and one microplate fixed. The higher frequency ratio for in-phase vibration is due to the absence of coupling effect of the spring's foundation between the two smart composite microplates. It is also concluded that the small scale effect in the case of in-phase vibration is higher than that in the out-of-phase vibration and one microplate fixed cases.
Obviously, increasing the μ^* increases the frequency ratio. This is due to the fact that the increase of nonlocal parameter decreases the interaction force between microplate atoms, and that leads to a softer structure.

Table 2 Comparing dimensionless nonlinear frequency obtained in the this study and those of Shen et al. [15]

Temperature		Ω_{NL}/Ω_L			
		$w/h=0.5$	$w/h=1$	$w/h=1.5$	$w/h=2$
T=300	**Present work**	1.0208	1.0802	1.1742	1.2933
	Shen et al. 2010	1.0205	1.0798	1.1720	1.2900
T=400	**Present work**	1.0339	1.1292	1.2738	1.4492
	Shen et al. 2010	1.0337	1.1289	1.2719	1.4485
T=500	**Present work**	1.0731	1.2668	1.5372	1.8498
	Shen et al. 2010	1.0728	1.2663	1.5355	1.8477

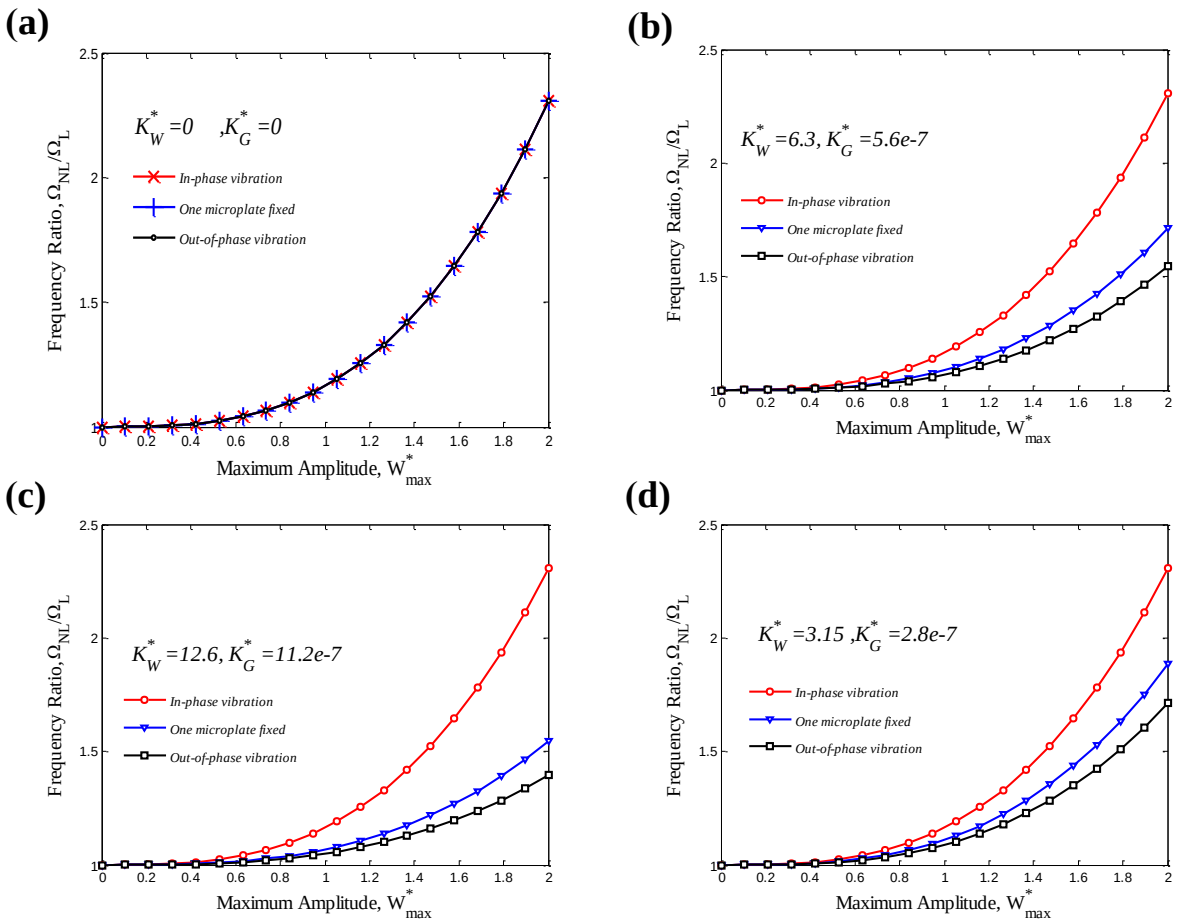

Figure 3 The effect of dimensionless coupling elastic medium on the frequency ratio versus the dimensionless maximum amplitude

The effect of geometrical aspect ratio (β_x) on the frequency ratio versus the dimensionless maximum amplitude for three different cases (i.e. out-of-phase, one microplate fixed and in-phase) is shown in figures (5a)-(5d). It is clear that the Ω_{NL}/Ω_L increases with increasing the $W^*_{\max}$ and the influence of three cases on the frequency ratio becomes more prominent at the higher dimensionless maximum amplitude. It is also found that the Ω_{NL}/Ω_L is decreased with increasing the β_x, since the equivalent stiffness of the system increases.

Furthermore, the difference between three cases of out-of-phase vibration, in-phase vibration and vibration with one microplate fixed becomes less at higher aspect ratio.

Hence, it can be concluded that with increasing geometrical aspect ratio, the effect of coupling elastic medium between two smart nano composite microplates reduces.

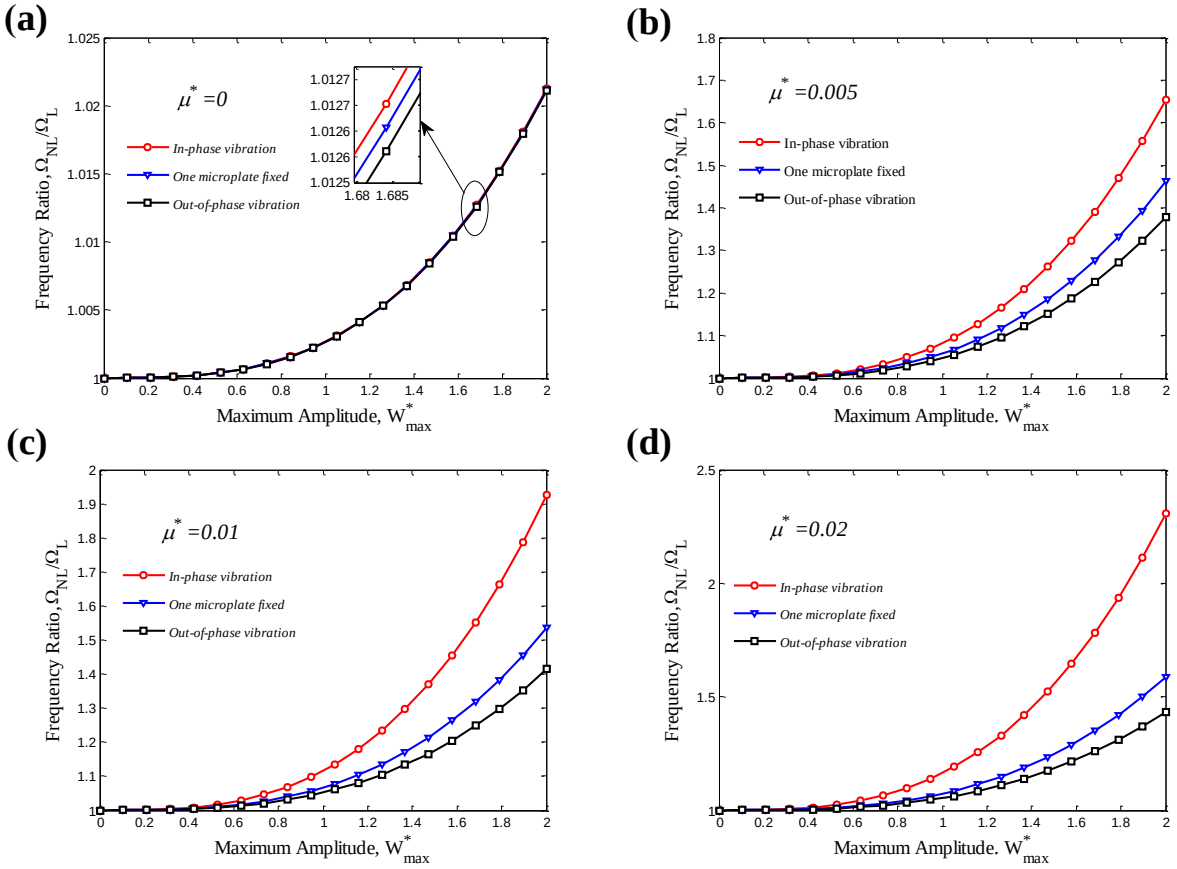

Figure 4 The effect of dimensionless nonlocal parameter on the frequency ratio versus the dimensionless maximum amplitude

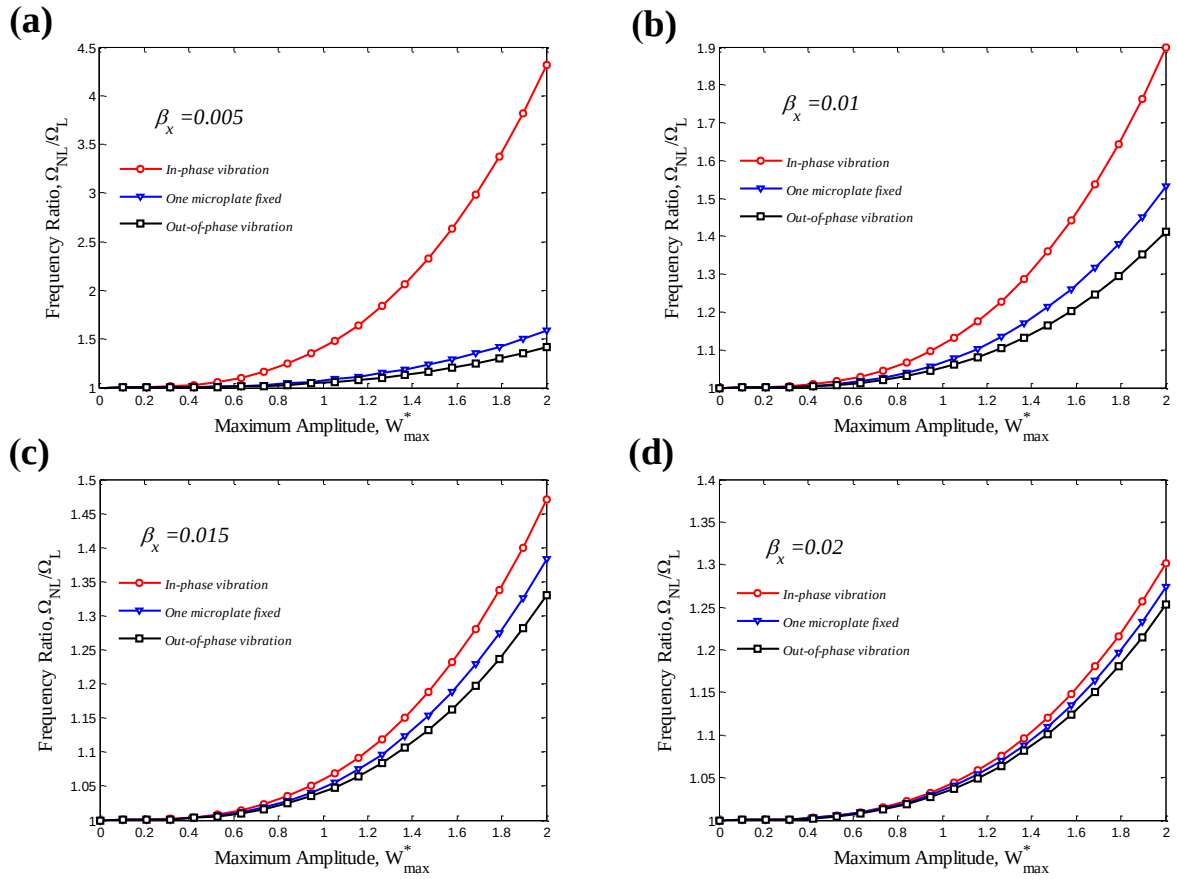

Figure 5 The effect of aspect ratio on the frequency ratio versus the dimensionless maximum amplitude.

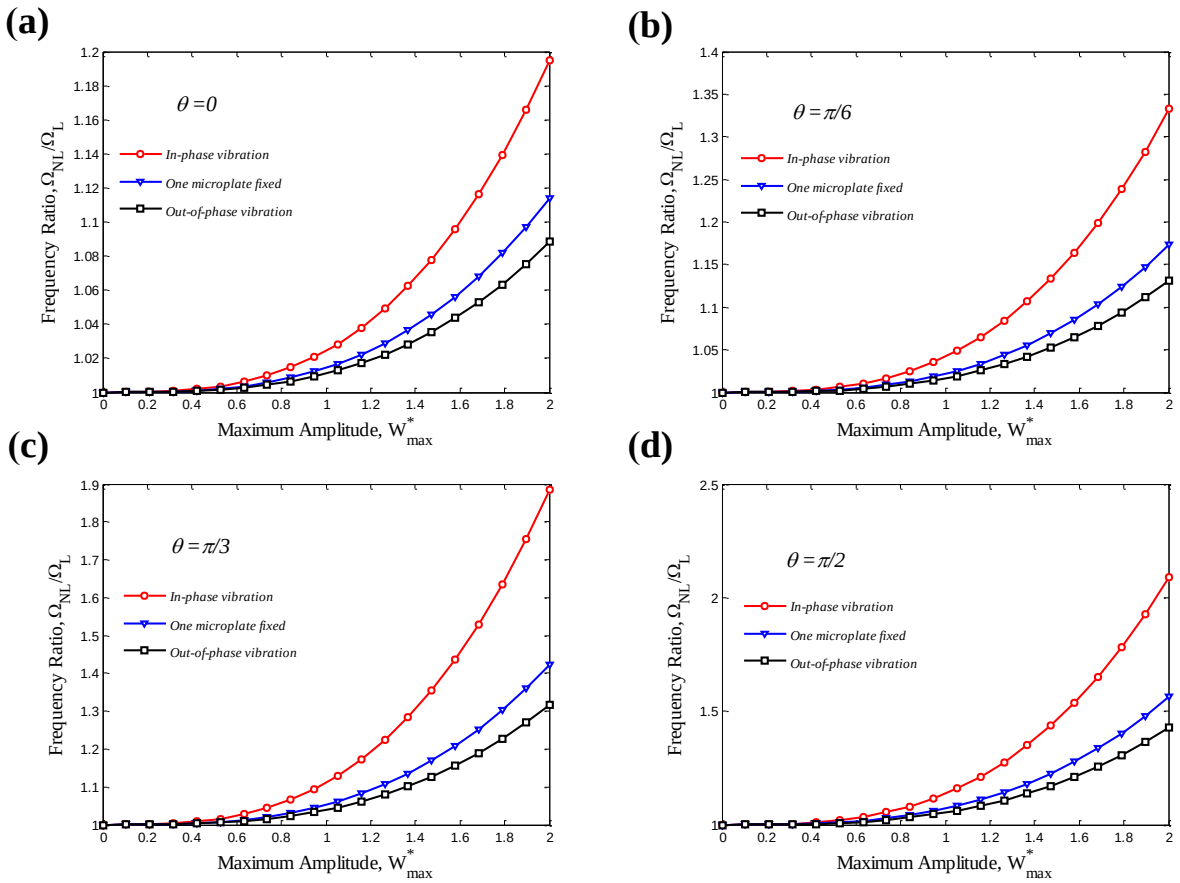

Figure 6 The effect of DWBNNT orientation angle in polymer on the frequency ratio versus the dimensionless maximum amplitude

Figures (6a)-(6d) demonstrates variations of the frequency ratio versus the dimensionless maximum amplitude for three different cases. Case 1, case 2 and case 3 represent the vibration in the states of out-of-phase, one microplate fixed and in-phase. Noted that figures (5a)-(5d) is plotted for different values of DWBNNT orientation angle in polymer which are taken as $\theta = 0$, $\theta = \pi/6$, $\theta = \pi/3$ and $\theta = \pi/2$, respectively. As can be seen Ω_{NL}/Ω_L is significantly dependent on θ so that the frequency ratio increases with increasing orientation angle. Moreover, frequency ratio of $\theta = \pi/2$ and $\theta = 0$ are maximum and minimum, respectively. This is most likely due to the fact that in $\theta = 0$, the direction of polarization for both reinforcements (DWBNNT) and matrix (PVDF) are the same which makes the system stiffer and leads to increase in frequency and consequently, decrease in frequency ratio. Comparing three cases mentioned above, it can be concluded that the effect of orientation angle on frequency ratio is remarkable at the in-phase vibration case. It is also observed that the difference between three cases becomes more distinguished at higher maximum amplitude. In realizing the influence of DWBNNT volume percent (ρ) in polymer, figures (7a)-(7d) indicates how frequency ratio changes with respect to the dimensionless maximum amplitude. Out-of-phase vibration, vibration with one microplate fixed and in-phase vibration is considered in this figure. Generally, the frequency ratio of the coupled system is decreased with increasing ρ. This is why, the Yong's modulus of reinforcer (e.g. DWBNNT) is much greater than polymer (e.g. PVDF). Therefore, with increasing ρ , elastic constants of the composite increase and consequently the smart composite microplates become more stable. The results indicate that increasing volume percent decreases the in-phase frequency ratio compared to the other cases. This is due to the absence of coupling effect of the elastic foundation between two microplates.

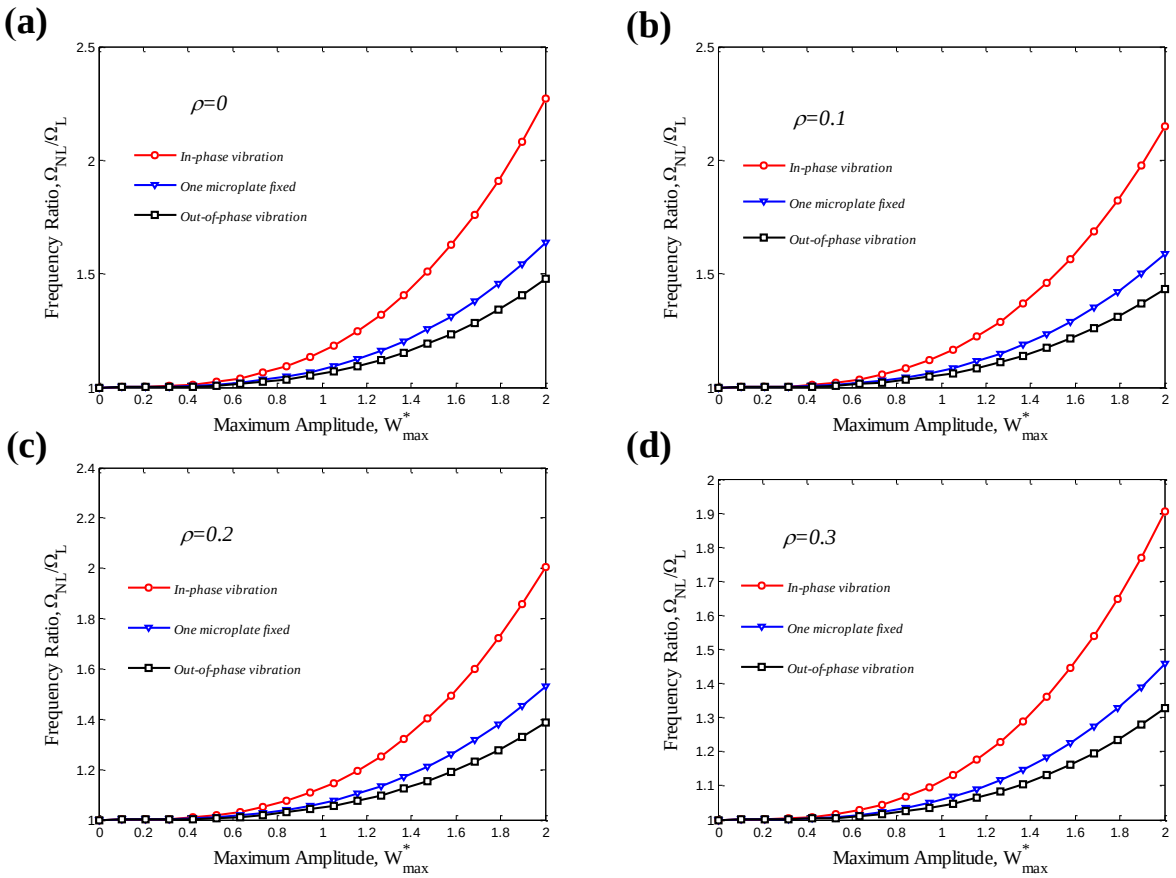

Figure 7 The effect of DWBNNT volume percent in polymer on the frequency ratio versus the dimensionless maximum amplitude

Figures (8a)-(8d) illustrates the influence of thermal gradient (ΔT) on the frequency ratio versus the dimensionless maximum amplitude. Here, similar to previous figures, three cases for vibration of the DPCMPS are considered. In three cases of out-of-phase vibration, vibration of one microplate fixed and in-phase vibration, it is evident that an increase in temperature change does not affect on the frequency ratio.

4 Conclusion

Vibration response of smart nano/micro composites have applications in designing many NEMS/MEMS devices such as hydraulic sensors and actuators. In the present study, electro-thermo nonlinear vibration of a double-smart composite microplate made of PVDF reinforced by DWBNNTs is investigated for three typical vibrational states, namely, out-of-phase, in-phase and the case when one microplate fixed. The internal elastic medium between two microplates is simulated as Pasternak foundation. Considering charge equation, the nonlinear motion equations are derived based on nonlocal piezoelasticity theory. The DQM is applied to obtain to the nonlinear frequency ratio of the DPCMPS so that the effects of the small scale coefficient, stiffness of the internal elastic medium, the volume fraction and orientation angle of the DWBNNTs reinforcement, temperature change and aspect ratio are discussed. The results of this study are validated by Shen et al. [15]. The results indicate that with increasing geometrical aspect ratio, the effect of coupling elastic medium between two smart ocomposite microplates decreases. Furthermore, the effects of small scale parameter, volume percent and orientation angle of DWBNNT in the case of in-phase vibration is higher than that in the out-of-phase vibration and one microplate fixed cases. It is also worth mentioning that the frequency ratio of the in-phase vibration is independent of elastic medium stiffness.

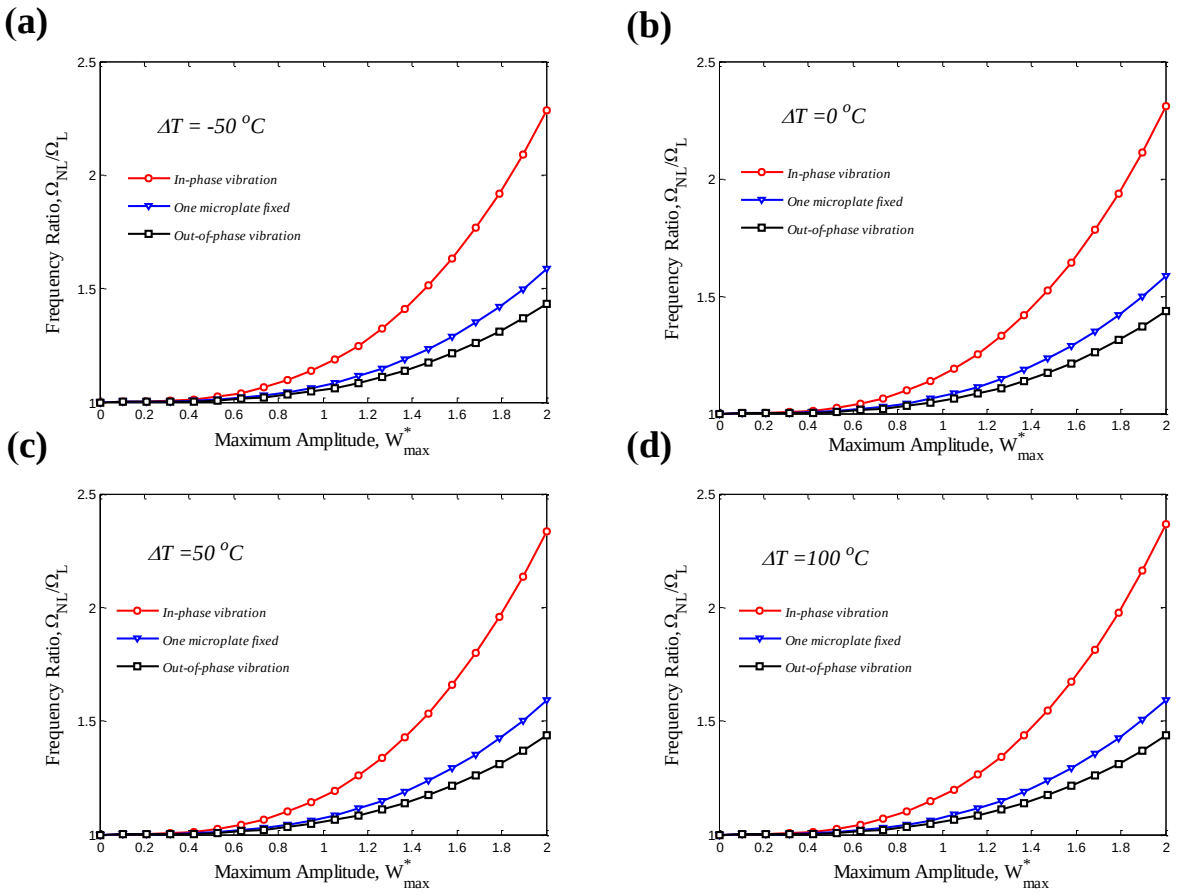

Figure 8 The effect of temperature change on the frequency ratio versus the dimensionless maximum amplitude.

Acknowledgments

The authors are grateful to University of Kashan for supporting this work by Grant No. 547600/8. They would also like to thank the Iranian Nanotechnology Development Committee for their financial support.

References

[1] Kotsilkova, R., "*Thermoset Nanocomposites for Engineering Applications*", Smithers Rapra Technology, UK, (2007).

[2] Merhari Hybrid, L., "*Nanocomposites for Nanotechnology*", Springer Science, New York, (2009).

[3] Schwartz, M., "*Smart Materials*", A Wiley-Interscience Publication Inc., New York, (2002).

[4] Yu, V., Christopher, T., and Bowen, R., "*Electromechanical Properties in Composites Based on Ferroelectrics*", Springer-Verlag, London, (2009).

[5] Vang, J., "*The Mechanics of Piezoelectric Structures*", World Scientific Publishing Co., USA, (2006).

[6] Vives, A.A., "*Piezoelectric Transducers and Applications*", Springer-Verlag Berlin, Heidelberg, (2008).

[7] Mosallaie Barzoki, A.A., Ghorbanpour Arani, A., Kolahchi, R., and Mozdianfard, M.R., "Electro-thermo-mechanical Torsional Buckling of a Piezoelectric Polymeric Cylindrical Shell Reinforced by DWBNNTs with an Elastic Core", Applied Mathematical Modelling, Vol. 36, pp. 2983–2995, (2012).

[8] Mosallaie Barzoki, A.A., Ghorbanpour Arani, A., Kolahchi, R., Mozdianfard, M.R., and Loghman, A., "Nonlinear Buckling Response of Embedded Piezoelectric Cylindrical Shell Reinforced with BNNT under Electro–thermo-mechanical Loadings using HDQM", Composite Part B, Vol. 44, pp. 722–727, (2012).

[9] Ghorbanpour Arani, A., Shajari, A.R., Amir, S., and Loghman, A., "Electro-thermo-mechanical Nonlinear Nonlocal Vibration and Instability of Embedded Micro-tube Reinforced by BNNT Conveying Fluid", Physica E, Vol. 45, pp. 109–121, (2012).

[10] Ghorbanpour Arani, A., Abdollahian, M., and Kolahchi, R., "Nonlinear Vibration of Embedded Smart Composite Microtube Conveying Fluid Based on Modified Couple Stress Theory", Polymer Composites, Vol. 36, pp. 1314–1324, (2015).

[11] Ghorbanpour Arani, A., Haghparast, E., Khoddami Maraghi, Z., and Amir, S., "Static Stress Analysis of Carbon Nano-tube Reinforced Composite (CNTRC) Cylinder under Non-axisymmetric Thermo-mechanical Loads and Uniform Electro-magnetic Fields", Composites Part B: Engineering, Vol. 68, pp. 136–145, (2015).

[12] Eringen, A.C., "*Nonlocal Polar Elastic Continua*", International Journal of Engineering Science, Vol. 10, pp. 1–16, (1972).

[13] Eringen, A.C., "*Nonlocal Continuum Field Theories*", Springer-Verlag, New York, (2002).

[14] Ghorbanpour Arani, A., Mosallaie Barzoki, A.A., Kolahchi, R., and Loghman, A., "Pasternak Foundation Effect on the Axial and Torsional Waves Propagation in Embedded Dwcnts using Nonlocal Elasticity Cylindrical Shell Theory", Journal of Mechanical Science and Technology, Vol. 25, pp. 2385-2391, (2011).

[15] Ghorbanpour Arani, A., and Jalaei, M.H., "Transient Behavior of an Orthotropic Graphene Sheet Resting on Orthotropic Visco-Pasternak Foundation", International Journal of Engineering Science, Vol. 103, pp. 97–113, (2016).

[16] Wang, Ch.Y., Li, X.H., and Luo, Y., "Circumferential Nonlocal Effect on the Buckling and Vibration of Nanotubes", Physics Letters A, Vol. 380, pp. 1455–1461, (2016).

[17] Zhang, Y., Zhang, L.W., Liew, K.M., and Yu, J.L., "Free Vibration Analysis of Bilayer Graphene Sheets Subjected to In-plane Magnetic Fields", Composite Structures. Vol. 144, pp. 86–95, (2016).

[18] Zhou, Z.G., and Wang, B., "The Scattering of Harmonic Elastic Anti-plane Shear Waves by a Griffith Crack in a Piezoelectric Material Plane by using the Non-local Theory", International Journal of Engineering Science, Vol. 40, pp. 303–317, (2002).

[19] Ke, L.L., Wang, Y.S., and Wang, Z.D., "Nonlinear Vibration of the Piezoelectric Nanobeams Based on the Nonlocal Theory", Composite Structures, Vol. 94, pp. 2038-2047, (2012).

[20] Ghorbanpour Arani, A., Fereidoon, A., and Kolahchi, R., "Nonlinear Surface and Nonlocal Piezoelasticity Theories for Vibration of Embedded Single-layer Boron Nitride Sheet using Harmonic Differential Quadrature and Differential Cubature Methods", Journal of Intelligent Material Systems and Structures, Vol. 26, pp. 1150–1163, (2015).

[21] Ghorbanpour Arani, A., Kolahchi, R., and Zarei, M.Sh., "Visco-surface-nonlocal Piezoelasticity Effects on Nonlinear Dynamic Stability of Graphene Sheets Integrated with Zno Sensors and Actuators using Refined Zigzag Theory", Composite Structures, Vol. 132, pp. 506–526, (2015).

[22] Murmu, T., and Adhikari, S., "Nonlocal Vibration of Bonded Double-nanoplate-systems", Composite Part B, Vol. 42, pp. 1901–1911, (2011).

[23] Murmu, T., Sienz, J., Adhikari, J., and Arnold, C., "Nonlocal Buckling Behavior of Bonded Double-nanoplate-systems", Journal of Applied Physics, Vol. 110, pp. 084316, (2011).

[24] Pouresmaeeli, S., Fazelzadeh, S.A., and Ghavanloo, E., "Exact Solution for Nonlocal Vibration of Double-orthotropic Nanoplates Embedded in Elastic Medium", Composite Part B, Vol. 43, pp. 3384–3390, (2012).

[25] Mohammadimehr, M., Rousta Navi, B., and Ghorbanpour Arani, A., "Free Vibration of Viscoelastic Double-bonded Polymeric Nanocomposite Plates Reinforced by FG-Swcnts using MSGT, Sinusoidal Shear Deformation Theory and Meshless Method", Composite Structures, Vol. 131, pp. 654–671, (2015).

[26] Ghorbanpour Arani, A., Kolahchi, R., and Vossough, H., "Buckling Analysis and Smart Control of SLGS using Elastically Coupled PVDF Nanoplate Based on the Nonlocal Mindlin Plate Theory", Physica B, Vol. 407, pp. 4458-4465, (2012).

[27] Vinson, J.R., "*Plate and Panel Structures of Isotropic, Composite and Piezoelectric Materials, Including Sandwich Construction*", Springer, USA, (2005).

[28] Reddy, J.N., "*Mechanics of Laminated Composite Plates, Theory and Analysis*", Chemical Rubber Company, Boca Raton, (1997).

[29] Tan, P., and Tong, L., "Micro-electromechanics Models for Piezoelectric-fiber-Reinforced Composite Materials", Composite Science and Technology, Vol. 61, pp. 759–769, (2001).

[30] Ghorbanpour Arani, A., Kolahchi, R., Mosallaie Barzoki, A.A., Mozdianfard, M.R., and Noudeh Farahani, S.M., "Elastic Foundation Effect on Nonlinear Thermo-vibration of Embedded Double-Layered Orthotropic Graphene Sheets using Differential Quadrature Method, Proceeding of IMech. Part C: Journal of Mechanical Engineering Science, Vol. 227, pp. 1-8, (2012).

Nomenclature

L	plate length
b	plate width
h	plate thickness
σ_{ij}^{nl}	nonlocal stress tensor
σ_{ij}^{l}	local stress tensor
D_k^{nl}	nonlocal electric displacement
D_k^{l}	local electric displacement
$\alpha(\lvert x-x'\rvert,\tau)$	nonlocal modulus
$\lvert x-x'\rvert$	Euclidean distance
l	external characteristic length
e_0	a constant appropriate to each material
a	internal characteristic length of the material
$\mu=(e_0 a)^2$	Nonlocal parameter
∇^2	Laplacian operator
u,v,w	total displacements of a point along the (x,y,z)
u_0,v_0,w_0	displacements of points on the mid-plane
$\varepsilon_{xx}^0,\varepsilon_{yy}^0,\gamma_{xy}^0$	components of the membrane strains
$\varepsilon_{xx}^1,\varepsilon_{yy}^1,\gamma_{xy}^1$	components of the bending strain
k_w	Winkler modulus
k_g	shear modulus
e_{ij}	piezoelectric constants
$\in_{ij}$	dielectric constants
α_k	thermal expansion coefficients
ΔT	temperature gradient
$\overline{C}_{ij}$	transformed stiffness components
C_{ij}	components of stiffness tensor
θ	orientation angle between the global and local Cartesian coordinates
E	electric field
ϕ	electric potential
δU	virtual strain energy
δV	virtual work done by external applied forces
δK	virtual kinetic energy
(m_0,m_2)	mass moments of inertia
ρ_0	plate density
(N_{xx},N_{yy},N_{xy})	force resultants
(M_{xx},M_{yy},M_{xy})	moment resultants
ω	frequency
C_{ij}^{ζ}	weighting coefficients

$M(\zeta_i)$	Lagrangian operators
$n_\zeta \times n_\eta$	grid points along x and y axes
$[M]$	mass matrix
$[K_L]$	linear stiffness matrix
$[K_{NL}]$	nonlinear stiffness matrix
Ω_{NL}	Dimensionless nonlinear frequency

چکیده

در این مقاله، ارتعاشات غیر خطی الکترو- ترمو- مکانیکی میکرو صفحه کامپوزیتی کوپله پیزوالکتریک بر اساس تئوری پیزوالاستیسیته غیر موضعی تحلیل و بررسی می گردد. دو صفحه نانوکامپوزیتی توسط محیط الاستیک که با محیط پاسترناک شبیه سازی شده است، به یکدیگر متصل شده است. هر دو صفحه از جنس پلیمر پلی وینیلیدن فلوراید بوده که با نانولوله های نیترید بور دو لایه تقویت شده است. مدل میکروالکترومکانیک برای بدست آوردن خواص معادل کامپوزیت استفاده شده است. با استفاده از روابط کرنش- تغییر مکانی غیر خطی و معادله شارژ برای کوپلینگ بین میدان های مکانیکی و الکتریکی، معادلات حرکت بر اساس روش انرژی و اصل همیلتون استخراج گردیده است. روش عددی تفاضلات مربعی برای حل معادلات حاکم و بدست آوردن فرکانس غیر خطی سازه استفاده شده است. نسبت فرکانس سیستم برای سه حالت ارتعاشات غیر هم فاز، هم فاز و حالتی که یکی از صفحات ثابت است، محاسبه شده است.

اثر پارامترهای مختلفی همچون پارامتر غیر موضعی، محیط الاستیک، درصد حجمی و زاویه چیدمان نانولوله ها، دما و پارامترهای هندسی روی نسبت فرکانس سیستم بررسی شده است. نتایج نشان می دهد که با افزایش پارامترهای هندسی، اثر محیط الاستیک بین صفحات کمتر می شود.